X-ray Spectroscopy of the Core of the Perseus Cluster with *Suzaku* : Elemental Abundances in the Intracluster Medium

T. Tamura, Y. Maeda, K. Mitsuda
Institute of Space and Astronautical Science, Japan Aerospace Exploration Agency, 3-1-1 Yoshinodai, Sagamihara, Kanagawa 229-8510, Japan

A. C. Fabian, J. S. Sanders
Institute of Astronomy, Madingley Road, Cambridge CB3 0HA, UK

A. Furuzawa
Department of Particle and Astrophysics, Nagoya University, Furo-cho, Chikusa-ku, Nagoya 464-8602, Japan

J. P. Hughes
Department of Physics and Astronomy, Rutgers University, Piscataway, NJ 08854-8019, USA

R. Iizuka
Department of Physics, Faculty of Science and Engineering, Chuo University, 1-13-27 Kasuga, Bunkyo-ku, Tokyo 112-8551, Japan

K. Matsushita
Department of Physics, Tokyo University of Science, 1-3 Kagurazaka, Shinjyuku-ku, Tokyo 162-8601, Japan
and

T. Tamagawa
RIKEN (Institute of Physical and Chemical Research), 2-1 Hirosawa, Wako, Saitama 351-0198, Japan

ABSTRACT

The results from *Suzaku* observations of the central region of the Perseus cluster are presented. Deep exposures with the X-ray Imaging Spectrometer provide high quality X-ray spectra from the intracluster medium. X-ray lines from helium-like Cr and Mn have been detected significantly for the first time in clusters. In addition, elemental abundances of Ne, Mg, Si, S, Ar, Ca, Fe, and Ni are accurately measured within $10'$ (or 220 kpc) from the cluster center. The relative abundance ratios are found to be within a range of $0.8 - 1.5$ times the solar value. These abundance ratios are compared with previous measurements, those in extremely metal-poor stars in the Galaxy, and theoretical models.

Subject headings: galaxies: clusters: general — X-rays: galaxies: clusters

1. INTRODUCTION

Heavy elements (or metals) in the universe are created in stars and supernovae (SNe). These metals enrich the interstellar medium and are recycled into generations of stars. Some part of these should have been transported into intergalactic space via galactic winds or ram pressure stripping. Indeed, the intracluster medium (ICM) contains an amount of metals comparable to the total amount of metals found in galaxies (e.g. Tsuru 1991). The distribution of these metals can be measured exclusively by X-ray spectroscopy. This constrains the total number of SNe in galaxies and the efficiency of the mass transport from galaxies into intergalactic space. Moreover, the abundance ratios among elements (e.g. Si/Fe ratio) can be used to identify their origins (e.g. Renzini et al. 1993).

ASCA and *Beppo-SAX* observations provided the first systematic measurements of Si, S and Fe abundances and their spatial distributions (e.g. Mushotzky et al. 1996). *XMM-Newton* has allowed more detailed studies including the O abundance determination (e.g. Tamura et al. 2004). Recent *Suzaku* data have further improved measurements of elements such as O and Mg (e.g. Matsushita et al. 2007). Mostly, observed abundance patterns are explained by some combinations of origins from type Ia and type II SNe (e.g. Fukazawa et al. 1998). Note that the nature of these SNe and hence their total metal products have not completely been understood. In addition, some authors claim that the observed metal abundances require an alternative source such as hypernovae in early generations of stars (Loewenstein 2001; Baumgartner et al. 2005). However, measurements are still limited to abundant elements and even for those elements statistical and systematic errors are large. See Böhringer & Werner (2009) for a recent review on X-ray spectroscopy of clusters.

Here we present *Suzaku* XIS (X-ray Imaging Spectrometer) spectroscopy of the central region of the Perseus cluster of galaxies, which is the brightest cluster in X-rays. This is a calibration target of the XIS and hence has been observed regularly. We used all available data from several exposures. The deep exposure of this unique object along with the high sensitivity of the XIS provides one of the best quality X-ray spectra from clusters. We have detected X-ray line emission from ionized Cr and Mn for the first time from an extragalactic source. Furthermore we accurately measured elemental abundances of Ne, Mg, Si, S, Ar, Ca, Fe, and Ni.

Throughout this paper, we assume cosmological parameters as follows; $H_0 = 70$ km s^{-1}Mpc^{-1}, $\Omega_{\rm m} = 0.3$, and $\Omega_\Lambda = 0.7$. At the cluster redshift of 0.0183, one arc-minute corresponds to 22.2 kpc at the cluster distance. We use the 90% confidence level.

2. OBSERVATIONS

As a calibration target, the Perseus cluster has been observed twice a year in various operation modes. Here we use the data obtained from February 2006 to February 2009 in the normal window mode. Sequence numbers of the data are 800010010, 101012010, 101012020, 102011010, 102012010, 103004010, 103005010, and 103004020. The central galaxy, NGC 1275, has been located at the CCD center. The detector covers a central $17' \times 17'$ square region. The XIS 2 sensor was available only until 2006. The cumulative exposure time in the spaced-row charge injection *off* mode is 300 ks times sensors (XIS 0, XIS 2, and XIS 3; FI)[1]. Those in the spaced-row charge injection *on* mode are 580 ks times sensors (FI) and 265 ks (XIS 1; BI). Detailed descriptions of the *Suzaku* observatory, the XIS instrument, and the X-ray telescope are found in Mitsuda et al. (2007), Koyama et al. (2007), Serlemitsos et al. (2007), respectively.

3. ANALYSIS AND RESULTS

3.1. Method

We started the analysis from archived cleaned event files, which were filtered with the standard selection criteria. We used the latest calibration file as of May 2009. We examined light curves excluding the central bright region events ($R < 6'$) for stable-background periods. There was no flaring event in all data. The instrumental (Non-X-ray) background was estimated using the night earth observation database and the soft-

[1] BI data in spaced-row charge injection off are not used.

ware `xisnxbgen` (Tawa et al. 2008). The cosmic X-ray background was estimated to be well below 1% of the source over almost entire enegy band. We therefore ignore this cosmic background in the following analysis.

We extracted spectra from three annulus regions with boundary radii of $0'.5$, $2'$, $4'.0$, and $10'$ centered on the X-ray maximum. The central region ($R < 0'.5$) is excluded to avoid the contribution from the central galaxy.

We prepared an X-ray telescope response function for each spectrum using the XIS ARF builder software `xissimarfgen` (Ishisaki et al. 2007), assuming an ICM surface brightness distribution based on an *XMM-Newton* public image of the cluster as a source image. We simulated events so that the relative error of the response at each energy bin is smaller than 0.25% (using a parameter `accuracy`). To made the XIS energy response function, we used the software `xisrmfgen`.

To describe the thermal emission from a collisional ionization equilibrium plasma, we use the APEC model (Smith & Brickhouse 2001) with the solar metal abundances taken from Anders & Grevesse (1989). The Galactic absorption is described by the photo-electric absorption of Wisconsin cross-sections (wabs model in XSPEC) with the reported neutral hydrogen column density of $1.5 \times 10^{-21}\mathrm{cm}^{-2}$ toward the cluster.

3.2. Spectral Fitting and Elemental Abundances

We fit the data to constrain the thermal nature and metal abundances. To describe the complex thermal structure of the central cooling core, projection effect, and photon mixing due to the point spread function, we introduce two thermal components. Temperatures and iron abundances of the two components are made independently free. On the contrary, other abundances of Ne, Mg, Si, S, Ar, Ca, and Ni are coupled between the two components, e.g. $\mathrm{Ne}_1 = \mathrm{Ne}_2$. A power-law component with a fixed photon index of 1.8 is also included. This describes a combination of scattering of the central galaxy emission and the possible distributed hard X-ray emission suggested by Sanders et al. (2004). In some spectra we found line emission at the position of He-like Cr. Because there is no line from Cr included in the APEC model, here, we add a Gaussian component for the Cr line into the fitting model. A detailed analysis of this line is given in the next subsection.

To avoid calibration errors, we ignore energy ranges around the Si K edge ($1.6 - 1.95$ keV) and the Au M edge ($2.2 - 2.4$ keV). To compensate errors of the energy-PI relation, redshifts of the two APEC components are allowed to be different. In $0'.5 - 2' - 4'$ regions, we use the FI and BI spectra simultaneously. In the $4' - 10'$ region, we use only the FI spectrum, since the BI spectrum has a relatively low signal to background ratio at higher energies, > 5 keV.

The fitting result is given in Table 1. Statistical errors of elemental abundances are $5 - 10\%$ of the best fit value. Obtained abundances are shown in Fig. 1(a). Here we use the Fe abundance averaged over those of the two components by weighting by the emission measure.

Examples of the spectral fitting are shown in Fig. 2. There are two types of systematic residuals. The one is those found around strong lines, such as the Fe K line at ~ 6.5 keV in the $0'.5 - 2'$ spectral fit. Limited accuracies in the energy response could cause these discrepancies. Furthermore, uncertainties in the modeling of the Fe K line structure could be larger than the statistics of the current data [2]. The other residual can be seen in the energy range of $5.5 - 7.5$ keV only in the $4'.0 - 10'$ fit. This could be related to instrumental background. At this energy band, the background is dominated by line emission such as Mn K_α (5.9 keV), Mn K_β (6.5 keV), and Ni K_α (7.5 keV). Time variations in line fluxes and changes in the line spread function create errors on the background estimation (Tawa et al. 2008). Nevertheless, each model describes the data with residuals smaller than five percent in most energy bins.

To estimate systematic errors associated with the instrumental calibration, we fit the FI and BI spectra separately and compare the results with those obtained from the combined (FI and BI) fits above. In these fits, statistical errors on abun-

[2] To assess possible uncertainties in the Fe K line modeling, we compared the APEC with the MEKAL model implemented in the XSPEC. After convolving models with the XIS response, we found differences between the two of $5 - 10\%$. A similar level of model uncertainties is expected.

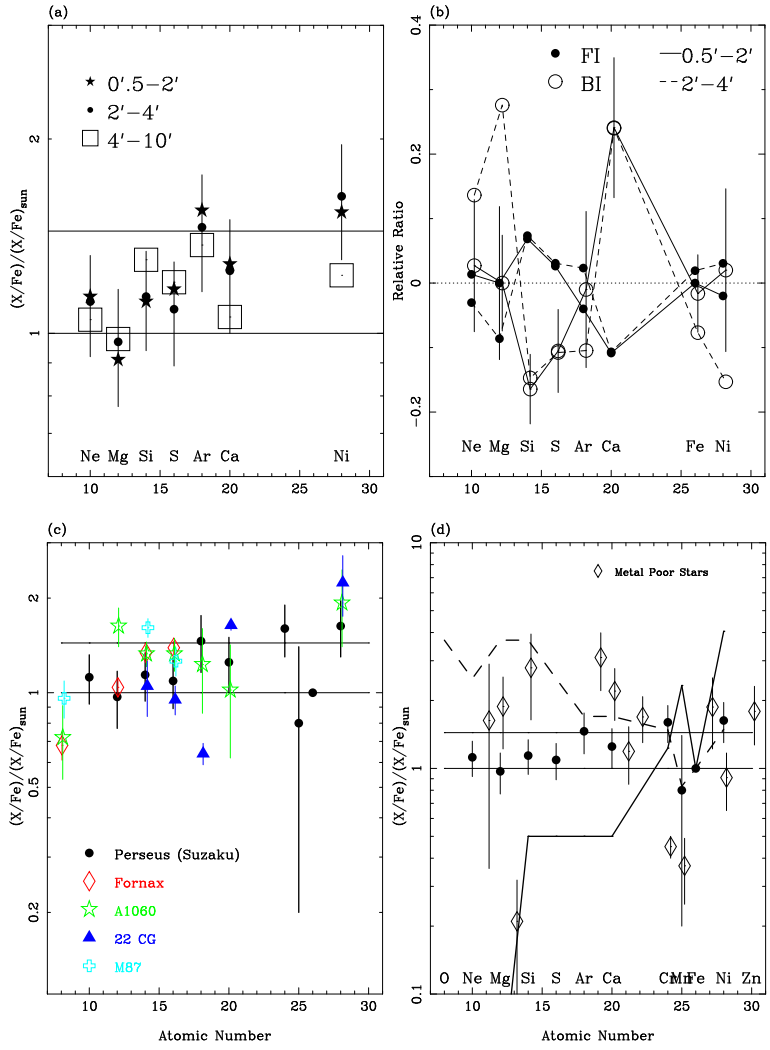

Fig. 1.— (a) Elemental abundance ratios determined from the two temperature fits. X/Fe (X=Ne, Mg, Si, S, Ar, Ca, and Ni) are shown in relative to those of the solar value (i.e. $(X/Fe)/(X/Fe)_{\odot}$). Typical errors are given for the $2' - 4'$ region. The Fe abundance is calculated by averaging over those of the two components. (b) Relative differences of the best fit parameters. Filled circles show differences between best-fit values obtained from the FI fit and those from the combined one (FI+BI) normalized by the latter value. Open circles show those from the BI fit. Points connected with solid- and dashed-lines are from the $0'.5 - 2'$ and $2' - 4'$ regions, respectively. Statistical errors are given only at the BI $0'.5 - 2'$ values. Compared with these errors, errors of other values are similar or small. (c) Comparison with previous X-ray measurements. Results of the Fornax cluster (Matsushita et al. 2003), A 1060 (Sato et al. 2007), average values of 22 clusters (de Plaa et al. 2007) and M87 (Matsushita et al. 2003) are shown along with the present result of the Perseus cluster ($2' - 4'$ region). The two vertical lines indicate 'photospheric' (1.0) and 'meteoritic' (1.44) solar abundances, corresponding to iron number density, Fe/H, of 4.68×10^{-5} and 3.24×10^{-5}, respectively. (d) Same for (c), but with abundances in extremely metal poor stars in the Galaxy (Cayrel et al. 2004). Predictions from type Ia and type II SNe are also shown in solid- and dashed-lines, respectively. Model yields are taken from Iwamoto et al. (1999) (W7 model for the type Ia).

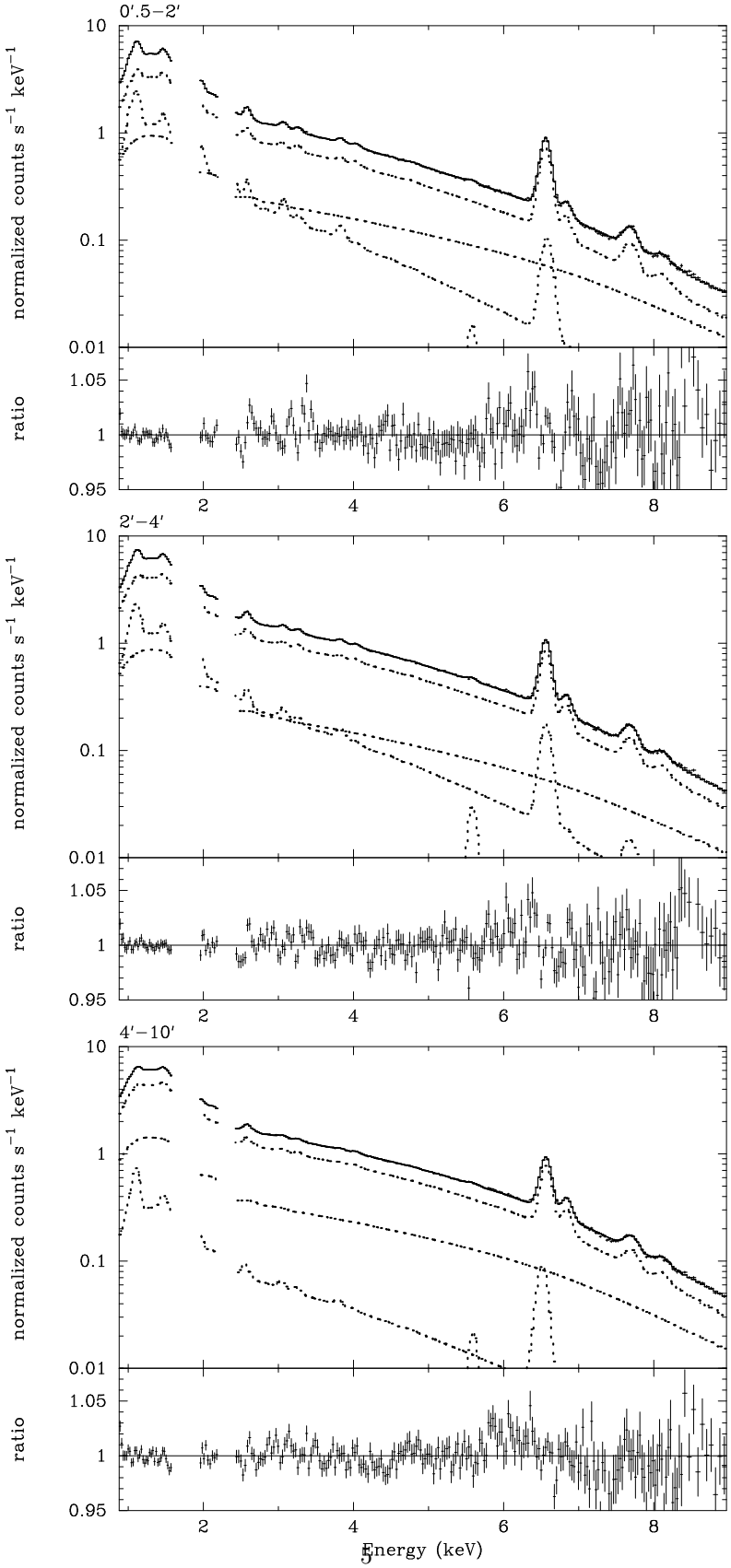

Fig. 2.— Cluster spectra along with the best-fit model. From top to bottom, the FI-CCD data from $0.5' - 2' - 4' - 10'$ regions are shown. The model components are shown by lines in upper panels. In lower panels fit residuals in terms of the data to model ratio are shown.

TABLE 1

THE FITTING RESULTS USING THE TWO TEMPERATURE COMPONENTS.

Region (radii)	XIS	$\chi^2/d.o.f.$	T1 (keV)	Fe1 (solar)	Norm1[a]	T2 (keV)	Fe2 (solar)	Norm2[a]	P-Norm[b]
$0'.5-2'$	FI+BI	1246/471	4.2 ± 0.04	0.62 ± 0.01	0.37 ± 0.01	2.2 ± 0.1	0.71 ± 0.02	0.13 ± 0.01	3.1 ± 0.1
$2'-4$	FI+BI	1207/471	5.0 ± 0.1	0.53 ± 0.01	0.39 ± 0.01	2.5 ± 0.05	0.83 ± 0.04	0.12 ± 0.01	2.5 ± 0.1
$4'-10'$	FI	485/239	5.7 ± 0.1	0.45 ± 0.01	0.56 ± 0.01	2.9 ± 0.1	1.5 ± 0.5	0.036 ± 0.01	4.9 ± 0.2

[a]Normalization of VAPEC component in the unit used in XSPEC.

[b]Normalization of the power-law component in unit of 10^{-2} photons keV^{-1} s^{-1} at 1 keV.

dances are about $5-10\%$ and $10-15\%$ for the FI and BI spectra, respectively. As shown in Fig. 1(b) relative differences between the separate and combined fits are within 20% mostly and within 30% in all cases. By this comparison and the current calibration status of the XIS[3], we suppose that the possible systematic errors on the abundances are about $\pm(20-30)\%$ of the best-fit values.

In the core of the Perseus cluster, resonant scattering may redistribute some Fe line photons spatially from the core to the outer region. We examined this effect by following Churazov et al. (2004). The resonant scattering should be relatively significant on the resonance transition of He-like Fe ($1s^2$-1s2p) at 6.70 keV. Then, we exclude this line energy band ($6.3-6.8$ keV) and fit the data again. This fit gives consistent abundances of Fe and Ni with the previous one. This indicates that the scattering is insignificant in our data. Using *XMM-Newton* data, Churazov et al. (2004) and Gastaldello & Molendi (2004) independently reported consistent results and suggested that the scattering effect is reduced because of gas motions in the core.

3.3. Cr and Mn Line emission

As mentioned above, we detected X-ray line emission from Cr. Next to Cr, we expect line emission from Mn from a sub-solar metallicity plasma. Note that the Cr and Mn solar abundances are about 1% and 0.5% of that of Fe, respectively. To search for these lines, we use the FI spectra integrated over a $0'.5-10'$ region in spaced-row charge injection *on* and *off* modes together. As shown in Fig. 3(a), by comparing the data with a bremsstrahlung continuum model, we have detected a line from He-like Cr clearly and that from He-like Mn. Note that in the model used in this fit the Si-escape line associated with the He-like Fe K_α line is included. This Si-escape line has a peak at 4.8 keV with a flux of about 1% of the data at that position.

Using the same data above and Gaussian line fitting, we measured these line positions and fluxes as given in Table 2. The detection of the Cr line is more than 99.9% confidence level, while that of the Mn line is more than 98% level. The fluxes are measured with respect to that of the He-like Fe K_α line at 6.70 keV. The resonance transitions of He-like Cr and Mn are at 5.682 keV and 6.181 keV, respectively (Hwang et al. 2000). The obtained line positions are fully consistent with those of redshifted resonance positions. The equivalent widths of the Cr and Mn lines are about 5 eV and 2 eV, respectively.

In a similar way as above, we examined spectra from the three regions separately. The significances of the Cr line detections are $>99.9\%$, $>99.9\%$, and 94% confidence from the $0'.5-2'-4'-10'$ spectra, respectively. The Mn line detection is significant ($>90\%$ confidence) only from the $0'.5-2'$ spectrum. In Table 2, we show the obtained line positions and fluxes.

To check if these features are instrumental, we examine the Crab nebula and instrumental background data obtained with the XIS. The Crab has a bright power-law X-ray emission and is a standard calibration source for X-ray instruments. In the Crab spectra, there is no structure at the line positions of Cr and Mn detected above. We found no structure at the same positions in the instrumental background. There are lines from neutral

[3]See "The Suzaku Technical Description" available at `http://www.astro.isas.jaxa.jp/suzaku/doc/suzaku_td/`.

Mn K_α (5.895 keV) and K_β (6.490 keV). However, these position are away from those of He-like Cr or Mn. Moreover, we confirmed that the *Chandra* deep spectrum ($\sim$1 Ms exposure) shows a line feature at the same Cr position with a flux consistent with the *Suzaku* data. These facts, redshifted line positions, and the obtained flux as expected from a sub-solar metallicity plasma (as calculated in discussion) indicate that we detected the Cr and Mn line emission from the cluster.

In our knowledge, this is the first significant detection of X-ray line emission of Cr and Mn ions from an extragalactic source. Werner et al. (2006) reported the detection of the same Cr line from the cluster 2A 0335+096 at the 2σ level.

4. SUMMARY AND DISCUSSION

Suzaku XIS observations of the Perseus cluster provided one of the best quality X-ray spectra from clusters. We have detected the He-like Cr and Mn lines. Furthermore, we measured the radial distribution of abundances of Ne, Mg, Si, S, Ar, Ca, Fe, and Ni. There is no strong radial variation in relative abundance ratios such as Mg/Fe and Si/Fe. The abundance ratios are within a range of $0.8-1.5$ times the solar value.

4.1. Cr and Mn abundances

Based on observed line fluxes of Cr and Mn ions, we estimate abundances of these elements. There is no atomic data in the ATOMDB (Smith & Brickhouse 2001) nor MEKAL (Kaastra 1992) providing X-ray emissivities of these lines. Then, following Hwang et al. (2000), we use line emissivities of elements (Si, S, Ar, Ca, Fe, and Ni) available from the ATOMDB and estimate those of Cr and Mn. Here we assume that emissivities per single ion of these elements at a given temperature is a smooth function of the atomic number. We interpolate the function using spline fits, as shown in Fig. 3(b). We used temperatures (Table 2) calculated by averaging over the two thermal components in the best-fit model obtained in subsection 3.2. Errors introduced by the interpolation would be smaller than $10-20\%$. This estimation along with observed fluxes gives Cr and Mn abundances (Table 2): Cr/Fe and Mn/Fe ratios are 1.6 ± 0.4 and 0.8 ± 0.6 times the solar, respectively.

The above estimated values obtained for Cr and Mn along with the Fe and Ni abundances derived in the spectral fitting provide iron-group abundances for the first time in the ICM. We found Cr:Mn:Fe:Ni ratios close to the solar value. These abundance patterns depend on the nature of their origins, supernovae (SNe). For example, Badenes et al. (2009) propose to reveal the detailed nature of type Ia SN using Mn, Cr, and Fe X-ray lines in SN remnants. In the case of the ICM metals, we can examine SNe averaged over many events in member galaxies. The present result supports the idea that the metals in the ICM and solar neighborhood were produced in a similar way.

4.2. Abundance Pattern

Our derived abundance pattern is compared with relevant observations and theories below. Some comparisons are shown in Fig. 1.

First, the *Chandra* result in the Perseus cluster (Sanders et al. 2004) is compared. We used their abundance pattern obtained from a region (40-80 kpc) similar to our data, but accounted for projection. The Ne/Fe, Si/Fe, Ar/Fe, Ca/Fe, and Ni/Fe ratios are consistent with the *Suzaku* result. In contrast, the *Chandra* data shows lower Mg/Fe (~0.5) and higher S/Fe ($1.5-1.8$) values than the solar ratio found in the current study. We suppose that these inconsistencies are caused partly by calibration errors used in Sanders et al. (2004) and partly caused by the difference in the spectral extraction method. Indeed, we found that much longer *Chandra* data ($\sim$ 1 Ms exposure) with the latest calibration and without the projection correction give Mg and S abundances consistent with our result.

Second, we compared our result with measurements in other clusters [Fig. 1(c)]. Note that including our study, most results are derived from cluster central regions (within a few 100 kpc). In most elements, our results are consistent with those in other clusters. Exceptions are lower Ar and higher Ca abundances in average values over a sample of 22 clusters reported by de Plaa et al. (2007). We cannot find this trend in the Perseus cluster. For all measured elements from Ne to Fe, the cluster abundances are consistent with the solar ratios within uncertainties. The Ni/Fe ratios are relatively high. This may be a sign of a con-

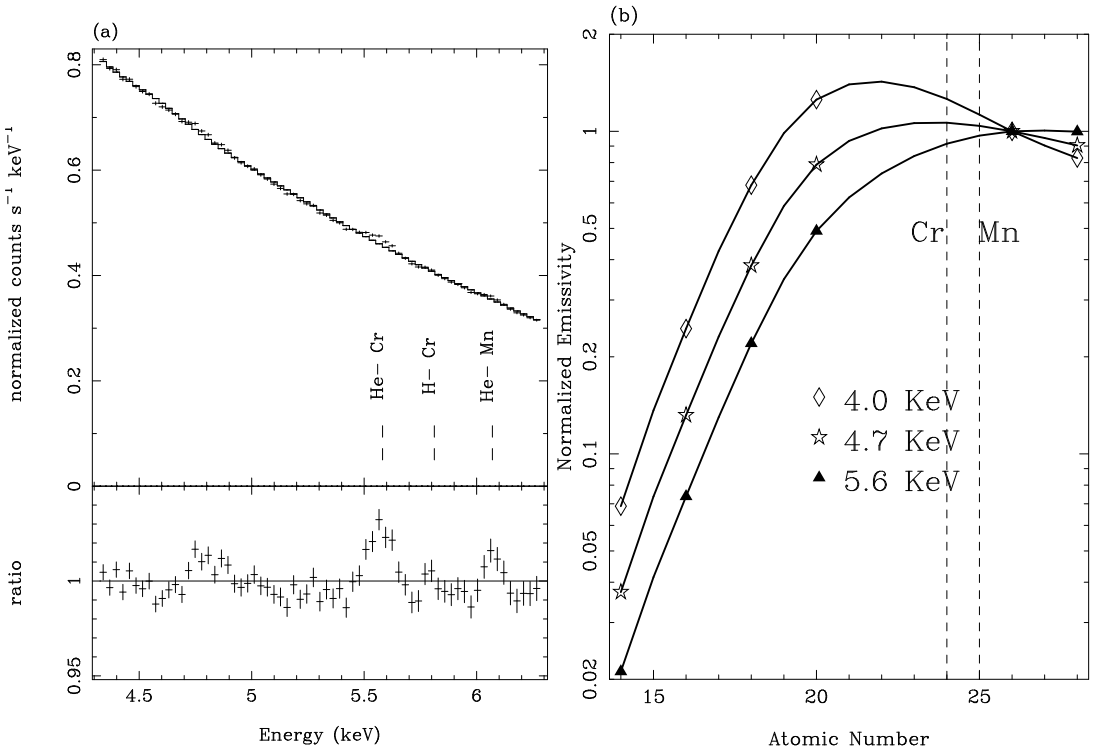

Fig. 3.— (a): Spectrum around the Cr and Mn lines extracted from the $0'.5 - 10'$ region. The FI CCD data with and without spaced-row charge injection are combined. The positions of He- and/or H-like Cr and Mn are indicated. (b): X-ray line emissivities from He-like ions as a function of the atomic number. The model values for Si, S, Ar, Ca, Fe, and Ni at three different temperatures obtained from the ATOMDB are shown by various mark points. Lines are spline fit to these values. Positions of Cr and Mn are indicated by dashed vertical lines.

TABLE 2

THE CR AND MN PARAMETERS OBTAINED FROM THE SPECTRAL FITTING.

Region	Cr position (eV)	Cr/Fe flux [a]	Mn position (eV)	Mn/Fe flux [a]	Cr/Fe ratio (solar) [b]	Mn/Fe ratio (solar) [b]	kT (keV)[c]
$0'.5 - 10'$	5574 ± 10	1.6 ± 0.3	6070±30	0.4 ± 0.2	–	–	–
$0'.5 - 2'$	5571 ± 35	1.81 ± 0.35	6070	0.49 ± 0.35	1.4 ± 0.3	0.8 ± 0.6	4.0
$2' - 4'$	5582 ± 30	1.76 ± 0.35	6070	0.41 ± 0.32	1.6 ± 0.3	0.8 ± 0.6	4.7
$4' - 10'$	5573 ± 40	1.53 ± 0.46	6070	$0.4(< 0.9)$	1.7 ± 0.5	$0.8(< 1.8)$	5.6

[a]Flux ratio to that of the He-like Fe K_α line at 6.7 keV in units of 10^{-2}.

[b]Elemental abundance ratio relative to the solar value.

[c]Assumed temperature.

tribution from type Ia SNe (e.g. Dupke & White 2000). The sub-solar value of O/Fe measured in other studies may have a similar origin (e.g. Tamura et al. 2001).

Third, our measurement is compared with that from Galactic stars with extremely low metallicity [Fig. 1(c); Cayrel et al. (2004)]. The latter abundances should be close to those originated from the first generation of stars and SNe in the universe. The patterns are very different. Among elements that we measured, elements lighter than Cr are more abundant in the metal poor stars, while Cr, Mn, and Ni are more abundant in the ICM. This comparison, regardless of theoretical models, indicates that the ICM is polluted not solely by the first generations of stars but also by additional source(s) significantly. The additional source(s) should add iron group elements to the ICM. The most-likely dominant contributor is type Ia SNe, as in the Galactic chemical evolution model (e.g. Kobayashi et al. 2006). The abundance pattern in the Perseus cluster is closer to the solar value than to those in extremely low metallicity stars. Therefore the contribution of the first generations of stars into the ICM metal is not required largely, in contrast to the model proposed in Loewenstein (2001).

Finally, the measured pattern is compared with theoretical predictions from two types of SNe [Fig 1(d)]. The observed abundance pattern cannot be produced solely by each type of SNe. All the observed abundance ratios are between the two predictions, except for Cr and Mn, which have relatively large uncertainties. Consequently, we conclude that the metals in the ICM of the Perseus and other clusters were produced by a mix of both types of SNe. Similar conclusions have been obtained from *ASCA* , *Chandra* , and *XMM-Newton* studies (e.g Fukazawa et al. 1998; Tamura et al. 2001; Sanders & Fabian 2006). The present data strengthen this scenario.

We thank J. S. Kaastra, K. Hayashida, and anonymous referee for their comments.

REFERENCES

Anders, E., & Grevesse, N. 1989, Geochimica et Cosmochimica Acta, 53, 197

Badenes, C., Bravo, E., and Hughese, J.P. 2009, ApJ, 680, L33

Baumgartner, W. H., Loewenstein, M., Horner, D. J., & Mushotzky, R. F. 2005, ApJ, 620, 680

Böhringer, H., & Werner, N. 2009, arXiv:0907.4277

Cayrel, R., et al. 2004, A&A, 416, 1117

Churazov, E., Forman, W., Jones, C., Sunyaev, R., Böhringer, H. 2004, MNRAS, 347, 29

Dupke, R. A., & White, R. E., III 2000, ApJ, 528, 139

Fukazawa, Y., Makishima, K., Tamura, T., Ezawa, H., Xu, H., Ikebe, Y., Kikuchi, K., & Ohashi, T. 1998, PASJ, 50, 187

Gastaldello, F. & Molendi, S. 2004, ApJ, 600, 670

Hwang, U., Petre, R., & Hughes, J.P., 2000, ApJ, 532, 970

Ishisaki, Y., et al. 2007, PASJ, 59, S113

Iwamoto, K., Brachwitz, F., Nomoto, K., Kishimoto, N., Umeda, H., Hix, W. R., & Thielemann, F.-K. 1999, ApJS, 125, 439

Kaastra, J.S. 1992, An X-Ray Spectral Code for Optically Thin Plasmas (Internal SRON-Leiden Report, updated version 2.0)

Kobayashi, C., Umeda, H., Nomoto, K., Tominaga, N., & Ohkubo, T. 2006, ApJ, 653, 1145

Koyama, K, et al. 2007, PASJ, 59, S23

Loewenstein, M. 2001, ApJ, 557, 573

Matsushita, K., Finoguenov, A., Böhringer, H. 2003, A&A, 401, 443

Matsushita, K. et al. 2007, PASJ, 59, 327

Mitsuda, K, et al. 2007, PASJ, 59, S1

Mushotzky, R., Loewenstein, M., Arnaud, K. A., Tamura, T., Fukazawa, Y., Matsushita, K., Kikuchi, K., & Hatsukade, I. 1996, ApJ, 466, 686

de Plaa, J., Werner, N., Bleeker, J. A. M., Vink, J., Kaastra, J. S., & Méndez, M. 2007, A&A, 465, 345

Renzini, A., Ciotti, L., D'Ercole, A. & Pellegrini, S., ApJ, 1993, 419

Sato, K. et al. 2007, PASJ, 59, 299

Sanders, J. S., Fabian, A. C., Allen, S. W., & Schmidt, R. W. 2004, MNRAS, 349, 952

Sanders, J. S., & Fabian, A. C. 2006, MNRAS, 371, 1483

Serlemitsos, P. et al. 2007, PASJ, 59, S9

Smith, R.K & Brickhouse, N.S. 2001, ApJ, 556, L91

Tawa, N., et al. 2008, PASJ, 60, 11

Tamura, T., Bleeker, J. A. M., Kaastra, J. S., Ferrigno, C., & Molendi, S. 2001, A&A, 379, 107

Tamura, T., Kaastra, J. S., den Herder, J. W. A., Bleeker, J. A. M., & Peterson, J. R. 2004, A&A, 420, 135

Tsuru, T. 1991, PhD thesis, University of Tokyo

Werner, N., et al. 2006, A&A, 449, 475

This 2-column preprint was prepared with the AAS LaTeX macros v5.2.